Journal of Dental Sciences 20 (2025) 510–521

Available online at www.sciencedirect.com

ScienceDirect

journal homepage: www.e-jds.com

Original Article

# Antimicrobial properties of bimetallic-containing mesoporous bioglass against *Enterococcus faecalis*

Kin-Weng Wong [a,1], Yi-Ju Li [a,1], Hui-Ci Yang [b], Chi-Sheng Chien [a,c], Li-Ting Kao [d], Ting-Sheng Lin [e,f], Tsung-Ying Yang [g,h,i,j**], Chi-Jen Shih [b,k,l*]

[a] *Department of Orthopedics, Chi Mei Medical Center, Tainan, Taiwan*
[b] *Department of Fragrance and Cosmetic Science, College of Pharmacy, Kaohsiung Medical University, Kaohsiung, Taiwan*
[c] *Department of Electrical Engineering, Southern Taiwan University of Science and Technology, Tainan, Taiwan*
[d] *Orthopaedic Research Center, College of Medicine, Kaohsiung Medical University, Kaohsiung, Taiwan*
[e] *Department of Biomedical Engineering, I-Shou University, Kaohsiung, Taiwan*
[f] *Biotechnology and Biomedical Engineering Center, I-Shou University, Kaohsiung, Taiwan*
[g] *Department of Medical Laboratory Science, I-Shou University, Kaohsiung, Taiwan*
[h] *Research Organization for Nano and Life Innovation, Future Innovation Institute, Waseda University, Tokyo, Japan*
[i] *Research Institute for Science and Engineering, Waseda University, Tokyo, Japan*
[j] *School of Education, Waseda University, Tokyo, Japan*
[k] *Drug Development and Value Creation Research Center, Kaohsiung Medical University, Kaohsiung, Taiwan*
[l] *Department of Medical Research, Kaohsiung Medical University Hospital, Kaohsiung, Taiwan*

Received 13 March 2024; Final revision received 29 April 2024
Available online 8 May 2024

**KEYWORDS**
Mesoporous bioactive glass;
Silver;
Copper;

**Abstract** *Background/purpose:*: Various pulp-covering materials offer advantages in regenerative root canal treatment, but each has limitations, highlighting the need for more effective antibacterial strategies for pulp repair and regeneration. Mesoporous bioactive glasses (MBG) show significant biological activity, making them valuable in tissue/dental repair. Silver-incorporated MBG exhibits promising antibacterial effects against various bacteria;

* Corresponding author. Department of Fragrance and Cosmetic Science, College of Pharmacy, Kaohsiung Medical University, No. 100, Shih-Chuan 1st Road, Sanmin Dist., Kaohsiung, 80708, Taiwan.
** Corresponding author. Department of Medical Laboratory Science, I-Shou University, No.8, Yida Road., Yanchao Dist., Kaohsiung City, 82445, Taiwan.
*E-mail addresses:* zegma040899@gmail.com (T.-Y. Yang), cjshih@kmu.edu.tw (C.-J. Shih).
[1] These authors contributed equally to this work.

https://doi.org/10.1016/j.jds.2024.04.029
1991-7902/© 2025 Association for Dental Sciences of the Republic of China. Publishing services by Elsevier B.V. This is an open access article under the CC BY-NC-ND license (http://creativecommons.org/licenses/by-nc-nd/4.0/).

*Enterococcus faecalis*;
Antibacterial

copper ions are crucial in regulating angiogenesis signals. Co-loading copper and silver in bioactive glasses has been explored to address clinical challenges. This study modified the preparation of silver-copper bimetallic mesoporous bioactive glass, analyzing their textural properties and antibacterial activity against *Enterococcus faecalis*.

*Materials and methods:* The silver-copper co-loaded bioactive glass (designated as AgCu/80S) was synthesized using a sol–gel technique with modifications. Textural analyses were carried out via X-ray diffraction, UV–Vis spectroscopy, Brunauer–Emmett–Teller analysis, and transmission electron microscope. The ion-releasing activity determined using inductively coupled plasma-mass spectrometry, and the antibacterial activity against *E. faecalis* was assessed through disk diffusion and kinetic bacterial growth curve.

*Results:* The modification led to weaker crystallization of calcium silicate, altering ion-releasing and antibacterial activities. Ag3Cu2/80S exhibited the highest released silver ion concentration at 112.6 ppm, with an inhibition zone of 9.09 ± 0.09 mm in disk diffusion assays. However, the inhibition zone of Ag2Cu3/80S was 9.92 ± 0.04 mm, implying that the antibacterial activity may not only be influenced by silver ions.

*Conclusion:* The AgCu/80S showed a potential antibacterial activity against *E. faecalis*, whereas further research on AgCu/80S glasses is necessary to optimize ion release conditions, assess bioactivities, and explore potential dental applications.

© 2025 Association for Dental Sciences of the Republic of China. Publishing services by Elsevier B.V. This is an open access article under the CC BY-NC-ND license (http://creativecommons.org/licenses/by-nc-nd/4.0/).

## Introduction

Recent research has highlighted that over 90% of adults suffer from diseases related to pulp infection,[1,2] such as dental caries and trauma, often caused by microbial infections like *Enterococcus faecalis*, *Streptococcus mutans*, and *Porphyromonas gingivalis*. Thus, effective removal of microorganisms from the oral cavity is crucial in root canal therapy. The failure in repeated endodontic treatments may be led by persistent bacteria, poor root canal cleaning and sealing, improper coronal sealing, or untreated root canals.[3] The microbiological analysis indicated specific bacteria prevalence in primary and secondary pulp infections, emphasizing the importance of addressing bacterial persistence in treatment.[4] Traditionally, root canal files and antibiotics were used to excise infected tissue;[5–7] however, this led to treatment failure and tooth extraction due to bacterial resistance and incomplete removal.[1,8,9] The regenerative root canal treatment offers an alternative, such as pulpotomy and apexogenesis, to promote the repair and regeneration of dental pulp tissue.[6,10–12] Commonly used pulp-covering materials, including calcium hydroxide, mineral trioxide aggregate (MTA), and biodentine, aimed to induce cell proliferation and repair dentin formation for pulp regeneration.[7,13,14] Calcium hydroxide, known for its antibacterial properties, has limitations such as degradation and incomplete bacterial inhibition.[15,16] Despite its excellent sealing and biocompatibility, MTA may not effectively inhibit certain bacteria like *E. faecalis*.[17] Biodentine, with rapid solidification properties, demonstrated bacteriostatic effects against *E. faecalis* but may pose challenges in clearing repeated infections due to its quick coagulation.[18] Collectively, while various pulp-covering materials offer advantages in regenerative root canal treatment, each has its limitations, emphasizing the need for further research to develop more effective antibacterial strategies for pulp repair and regeneration.

The mesoporous bioactive glasses (MBG) synthesized via the sol–gel method with surfactants as structural guide agents exhibit remarkable biological activity, making them valuable in bone tissue regeneration and dental repair materials.[19,20] MBGs offer characteristics of high surface area, pore volume, and an ordered mesoporous structure, enabling the loading of functional ingredients such as drugs and metals for controlled release, which makes them versatile for various biomedical applications.[19,20] Silver ions ($Ag^{+}$) are well-known for their excellent antibacterial properties against both Gram-negative and Gram-positive bacteria;[21] silver nanoparticles (AgNPs) also exhibit remarkable antibacterial abilities and are less prone to causing microbial resistance. The previous studies have demonstrated the antibacterial efficacy of the silver-incorporated MBG (Ag-MBG) against bacteria like *Enterococcus coli* and *Staphylococcus* species,[22–24] with Ag-MBG showing significant inhibition zones, particularly against Gram-positive bacteria, *S. carnosus*.[23] The approaches have been taken to develop antibacterial bone scaffolds using Ag-MBG combined with materials like poly L-lactic acid (PLLA) or through 3D printing techniques.[22,24] The observations have shown promising antibacterial effects of Ag-MBG against various bacterial strains, making them potential candidates for bone or dental tissue engineering applications. Additionally, copper ions ($Cu^{2+}$) are recognized for their role in regulating angiogenesis signals,[25] promoting vascular endothelial cell proliferation, migration, and wound healing. The synergy effect between copper and silver ions on the antibacterial effect has been studied,[26,27] The previous study showed that combining copper oxide (CuO) nanoparticles with silver (Ag) nanoparticles significantly enhanced antibacterial properties,[26] with CuO nanoparticles boosting the antibacterial effect of Ag

nanoparticles up to 6 times. In another study, Hao et al. described that the silver-copper bimetallic nanoparticles (Ag—Cu NPs) effectively reduced the genotoxicity associated with individual nanoparticles while considerably enhancing their antibacterial efficacy.[27] The Ag—Cu NPs were noted for their synergistic effects on reactive oxygen species (ROS) generation processes, photocatalytic properties, antibacterial mechanisms, and the factors influencing their performance. These observations highlighted the potential of silver and copper combinations to enhance efficacy, reduce toxicity, and find broader applications.

A few efforts have been made on co-loading copper and silver in bioactive glasses to explore their multifunctionality in addressing clinical challenges.[28,29] The previous studies reported enhanced antibacterial properties against methicillin-resistant *Staphylococcus aureus* and vancomycin-intermediate *S. aureus*,[29] as well as promoting angiogenesis, as evidenced by increased wound healing rates and blood vessel formation.[28] These findings encouraged further research in silver and copper co-doped materials to develop novel therapeutic strategies for various biomedical applications, such as in the dental field. Hence, to better understand and improve the AgCu/80S materials, this study endeavored to modify the preparation of the silver-copper bimetallic mesoporous bioactive glass, making the AgCu/80S materials closer to a non-crystal bioglass. The textural analyses were carried out using ultraviolet—visible spectroscopy, Brunauer—Emmett—Teller analysis, transmission electron microscope, and inductively coupled plasma-mass spectrometry. The antibacterial activity of AgCu/80S against *E. faecalis* was also assessed via disk diffusion, kinetic growth curve, and colony-forming testing assays.

## Materials and methods

### Preparation of AgCu/80S materials

The silver-copper co-loaded bioactive glass (designated as AgCu/80S) was produced using a sol—gel technique as described in the previous study but with modifications.[29] Briefly, the composition of the material was $80SiO_2$—$15CaO$—$5P_2O_5$-(5-x)Ag-xCuO, where x signified the additional mole ratio with values ranging from 0 to 5. The tetraethyl orthosilicate (TEOS) (Acros, NJ, USA), triethyl phosphate (TEP) (Fluka, NC, USA), and calcium nitrate tetrahydrate ($Ca(NO_3)_2 \cdot 4H_2O$) (Showa, Osaka, Japan) were employed as precursors, with the addition of nitric acid (Showa) at 2M and Pluronic F-127 (BASF, Frankfurt, Germany) in 99.5% absolute ethanol. Silver nitrate ($AgNO_3$) (Showa) and copper nitrate trihydrate ($Cu(NO_3)_2 \cdot 3H_2O$) (Showa) were poured based on the composition ratio. The mixture was stirred at room temperature for 24h to generate the sol. Subsequently, polyurethane (PUF) (Nanapo, Kaohsiung, Taiwan) was utilized as a template, which was compressed and immersed in the sol for 1 min to facilitate the infiltration of the sol into its structure. The immersed PUF was placed at room temperature for 10 min, and the steps above were repeated twice. Aging was conducted by drying in an oven at 100 °C for 24 h to induce evaporation-induced self-assembly (EISA). Finally, the materials were placed in a high-temperature calcining furnace, with the heating rate at 10 °C/min up to 650 °C, and the temperature was maintained for 5 h to undergo thermal treatment for the removal of the template and surfactant, resulting in the production of AgCu/80S powder.

### X-ray diffraction

The powder of AgCu/80S material was placed on the platform and subjected to analysis utilizing an X-ray diffraction analyzer (Shimadzu XRD-6000; Kyoto, Japan) employing Cu K$\alpha$ rays ($\lambda$ = 1.542 Å). The angular range of measurement was $2\theta$ = 20—80°, the scanning velocity was set at 2°/min, and the Jade 6 software was utilized to compare the obtained data with the Joint Committee on Powder Diffraction Standards (JCPDS) database in order to validate the crystal structure corresponding to AgCu/80S.

### Ultraviolet—visible spectroscopy

An ultraviolet—visible spectrometer (Shimadzu UV-2600; Kyoto, Japan) was employed to detect the absorbance within 200—800 nm wavelength for the AgCu/80S powder to identify the metal nanoparticles in materials. Various materials exhibited distinct absorption wavelengths, and nanometals smaller than a certain size demonstrated a surface plasmon resonance phenomenon,[30] which subsequently produced characteristic absorption peaks under UV—Vis light irradiation.

### Brunauer—Emmett—Teller analysis

The nitrogen adsorption isotherm (Micromeritics ASAP 2020) was employed to assess the surface area, pore volume, and pore size distribution of AgCu/80S porous materials. The nitrogen at a specific partial pressure could help forming a monolayer on the material's surface and porous structures due to the van der Waals force. The specific surface area, pore volume, and pore size of the materials could be calculated as previously described.[31]

### Transmission electron microscope

The samples were prepared by spraying the materials in sterile distilled water onto the sample holder. The sample holders were dried at 60 °C for 5 days. A transmission electron microscope (JEOL JEM-3010; Tokyo, Japan) at an accelerating voltage of 200 kV was utilized to examine the morphology of the materials. A lanthanum hexaboride ($LaB_6$) filament within a vacuum system was employed to permeate the sample film with a high-energy electron beam, thus producing both a penetrating electron beam and a scattered electron beam. Subsequently, the electromagnetic lens is employed to amplify and concentrate these beams, resulting in diverse diffraction patterns or luminous and shadowy contrast imaging that facilitate the observation of the mesoporous structure of the substance.

### Inductively coupled plasma-mass spectrometry

An ICP-MS (iCAP TQ, Thermo Fisher Scientific) was employed to examine the silver and copper content in the inspired AgCu/80S solutions. The AgCu/80S materials were immersed in brain heart infusion (BHI, Himedia) broth, the bacterial culture medium used in this study, and shaken at 160 rpm and 37 °C for 24h, with 40 mg/mL solid—liquid ratio. After the centrifugation, a 0.22 μm filter was utilized to remove the solid powder in the supernatant. The filtered samples were then subjected to the ICP-MS detection.

### Disk diffusion assay

The AgCu/80S materials were pressed into tablets with a diameter of 8 mm. The bacterial suspension at $2 \times 10^8$ colony-forming units per milliliter (CFU/mL) of *E. faecalis* ATCC29212 was prepared and spread onto BHI agar using a swab. The 8-mm material tablets were gently placed on the bacterial lawn. The plate was incubated at 37 °C for 24h in an atmospheric environment. The diameter of the inhibition zone was measured. All experiments were repeated three times.

### Bacterial growth curve assay

The bacterial suspension at $2 \times 10^8$ CFU/mL was prepared, diluted 200 times, and added to a 96-well plate. Subsequently, various solid—liquid ratios of inspired AgCu/80S ranging from 1.25 to 40 mg/mL were also mixed, generating final concentrations ranging from 0.625 to 20 mg/mL and $5 \times 10^5$ CFU/mL. The 96-well plate was incubated at 37 °C in an atmospheric environment, and the absorbance value was measured hourly for 24h at a wavelength of 600 nm using a Microplate reader (Infinite F50). The minimum inhibitory concentration (MIC) was determined as the lowest concentration, observing no growth.

### Colony-forming assay

To further evaluate the minimum bactericidal concentration (MBC) of AgCu/80S against *E. faecalis*, the samples were collected from the 96-well plates for bacterial growth curve assays. A sterilized cotton swab was immersed into the sample and spread the sample onto BHI agar. The agar plates were incubated at 37 °C for 24h in an atmospheric environment. The concentration without a viable colony was regarded as the MBC.

## Results

### Crystal phase analysis of AgCu/80S

The crystallographic characteristics of AgCu/80S were determined using an X-ray diffraction analyzer to analyze the material at $2\theta = 20—80°$ to observe the crystal phase composition, with the Jade 6 software and JCPDS database employed for comparison (Fig. 1). All materials in this study exhibited the presence of glass ceramics containing calcium silicate crystals ($Ca_2SiO_4$) on planes of (301) (JCPDS

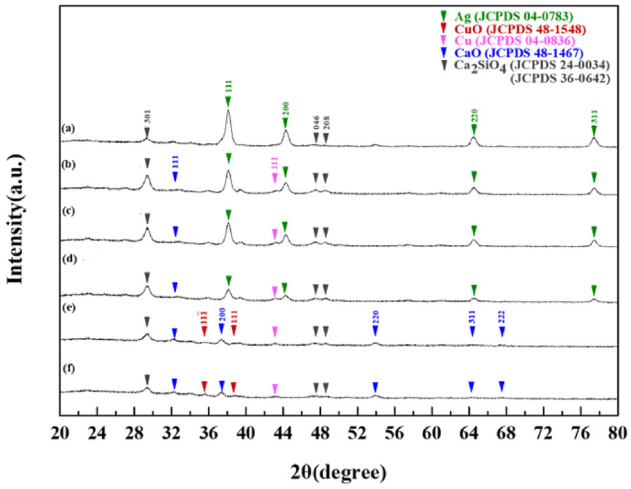


**Figure 1** X-ray diffraction results of (a)Ag5/80S, (b)Ag4Cu1/80S, (c)Ag3Cu2/80S, (d)Ag2Cu3/80S, (e)Ag1Cu4/80S, and (f) Cu5/80S.

24—0034) and planes of (046) and (208) (JCPDS 36—0642). The diffraction peaks of silver (Ag, JCPDS 04—0783) at $2\theta = 38.11°$, 44.27°, 64.47°, and 77.47° were noted in those materials containing Ag (Fig. 1a—e), with the crystal planes of (111), (200), (220), and (311), respectively. The signals increased as the concentration of Ag added increased. Similarly, the copper-containing materials (Fig. 1b—f) exhibited the crystallization of copper (Cu, JCPDS 04—0836) at $2\theta = 43.29°$ on the plane of (111). Furthermore, the crystal phase of copper oxide (CuO, JCPDS 48—1548) was observed at $2\theta = 35.54°$ and 38.70°, manifesting as (11-1) and (111), respectively, when the mole ratio of copper increased. The crystallization of calcium oxide (CaO, JCPDS 48—1467) was observed at $2\theta = 32.19°$, 37.35°, 53.85°, 64.15°, and 67.37°, with the resulting crystal faces being (111), (200), (220), (311), and (222). It was postulated that $Cu^{2+}$ infiltrated the material structure and replaced the position of $Ca^{2+}$ as more copper was added, resulting in CaO.

The ultraviolet spectrometer (UV—vis) was used to analyze materials for silver and copper crystal phases, with wavelengths ranging from 200 to 800 nm (Fig. 2). No characteristic absorption peak was detected in the 80S material, while the Ag5/80S, Ag4Cu1/80S, Ag3Cu2/80S, and Ag2Cu3/80S materials were observed with the of Ag nanoparticles at a wavelength near 400 nm. However, no related signal was observed in Ag1Cu4/80S, probably due to the low addition amount of silver. Additionally, no copper crystals were found in all compositions.

### Pore analysis of AgCu/80S

The mesoporous characteristics and pore size of AgCu/80S, with the 80S serving as a control group, were investigated to determine whether the addition of silver and copper to the material would impact the material properties (Fig. 3). According to the IUPAC classification, the adsorption and desorption curve of the 80S corresponds to a type IV H1 isotherm curve with a hysteresis loop, signifying

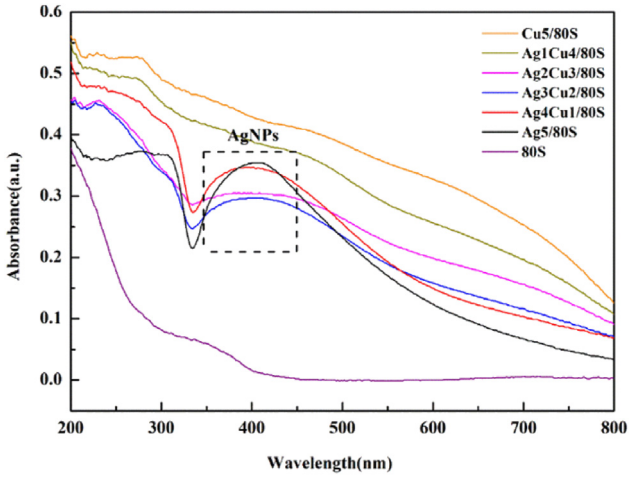


**Figure 2** UV—vis spectra of 80S, Ag5/80S, Ag4Cu1/80S, Ag3Cu2/80S, Ag2Cu3/80S, Ag1Cu4/80S, and Cu5/80S.

mesoporous materials, with a specific surface area and pore volume of 294.1 $m^2/g$ and 0.51 $cm^3/g$, respectively, and a pore size of 7.6 nm (Fig. 3a). The measurement aligned with the pore size of mesoporous bioactive glass, which falls within the range of 2—50 nm. The Ag5/80S, Ag4Cu1/80S, Ag3Cu2/80S, Ag2Cu3/80S, Ag1Cu4/80S, and Cu5/80S materials exhibited a notably smaller surface area and pore volume compared to 80S, where the values were 154.9 $m^2/g$ and 0.33 $cm^3/g$, 175.9 $m^2/g$ and 0.33 $cm^3/g$, 157.4 $m^2/g$ and 0.31 $cm^3/g$, 170.7 $m^2/g$ and 0.32 $cm^3/g$, 173.2 $m^2/g$ and 0.33 $cm^3/g$, 150.2 $m^2/g$ and 0.35 $cm^3/g$, respectively (Fig. 3b—g). The percentage of decreases in surface area ranged from 40.2% to 48.9%, and that in pore volume were from 31.4% to 39.2%, with the pore size of 7.4—9.1 nm (Table 1). Our findings suggested that silver and copper have indeed infiltrated the material, resulting in a decrease in surface area and pore volume.

## Morphology of AgCu/80S

The transmission electron microscope was employed to examine bright and dark field images to observe the morphology of the materials (Fig. 4). The Ag5/80S, Ag4Cu1/80S, Ag3Cu2/80S, Ag2Cu3/80S, Ag1Cu4/80S, and Cu5/80S exhibited an orderly disposition with lines, whereas the pores were found in a hexagonal form. Although the mesoporous structures were found no difference between 80S and AgCu/80S materials, the incorporation of silver and

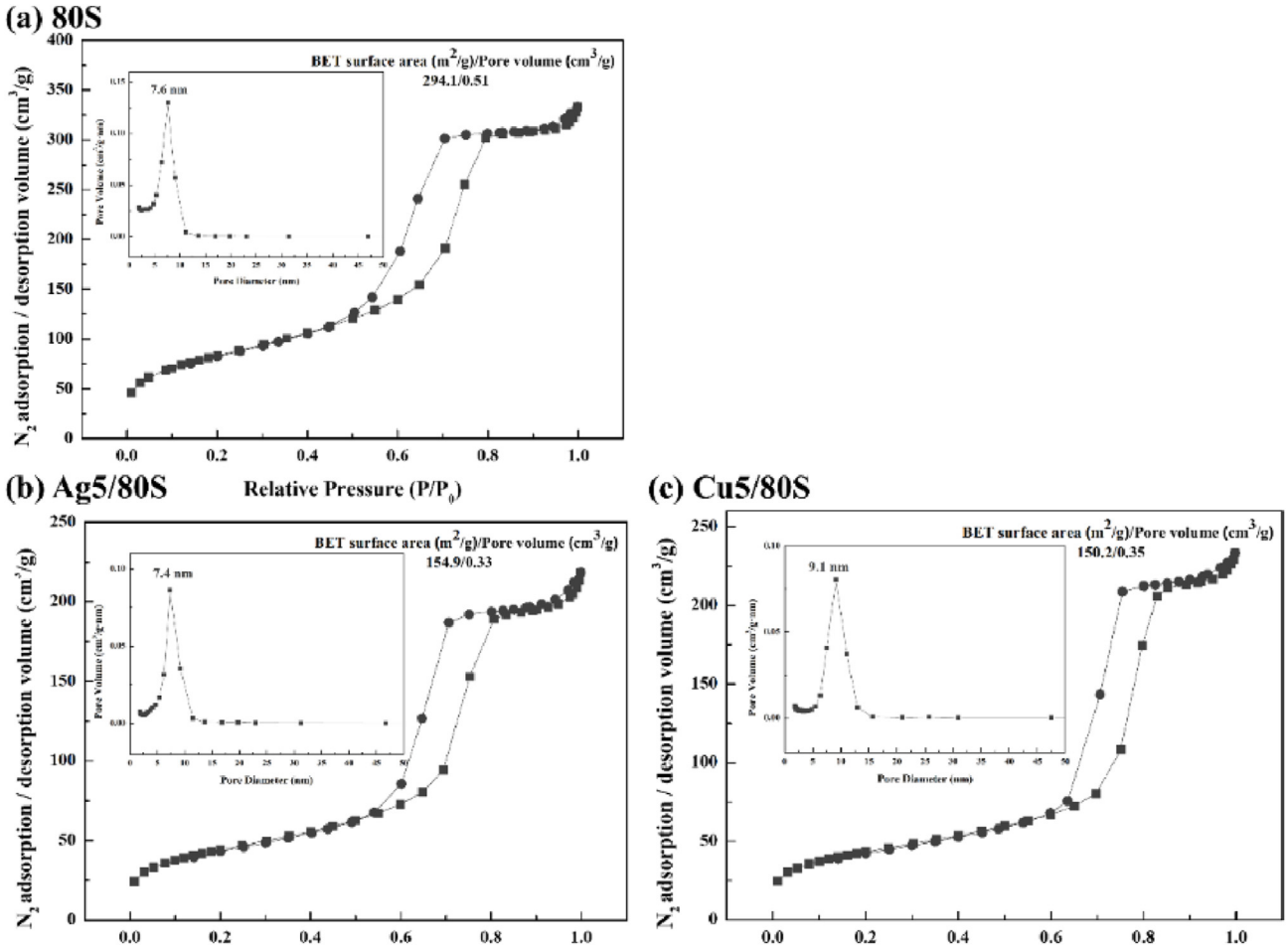


**Figure 3** Nitrogen adsorption/desorption isotherm and pore size distribution curve results of (a)80S, (b)Ag5/80S, (c)Cu5/80S, (d) Ag4Cu1/80S, (e)Ag3Cu2/80S, (f)Ag2Cu3/80S, and (g)Ag1Cu4/80S.

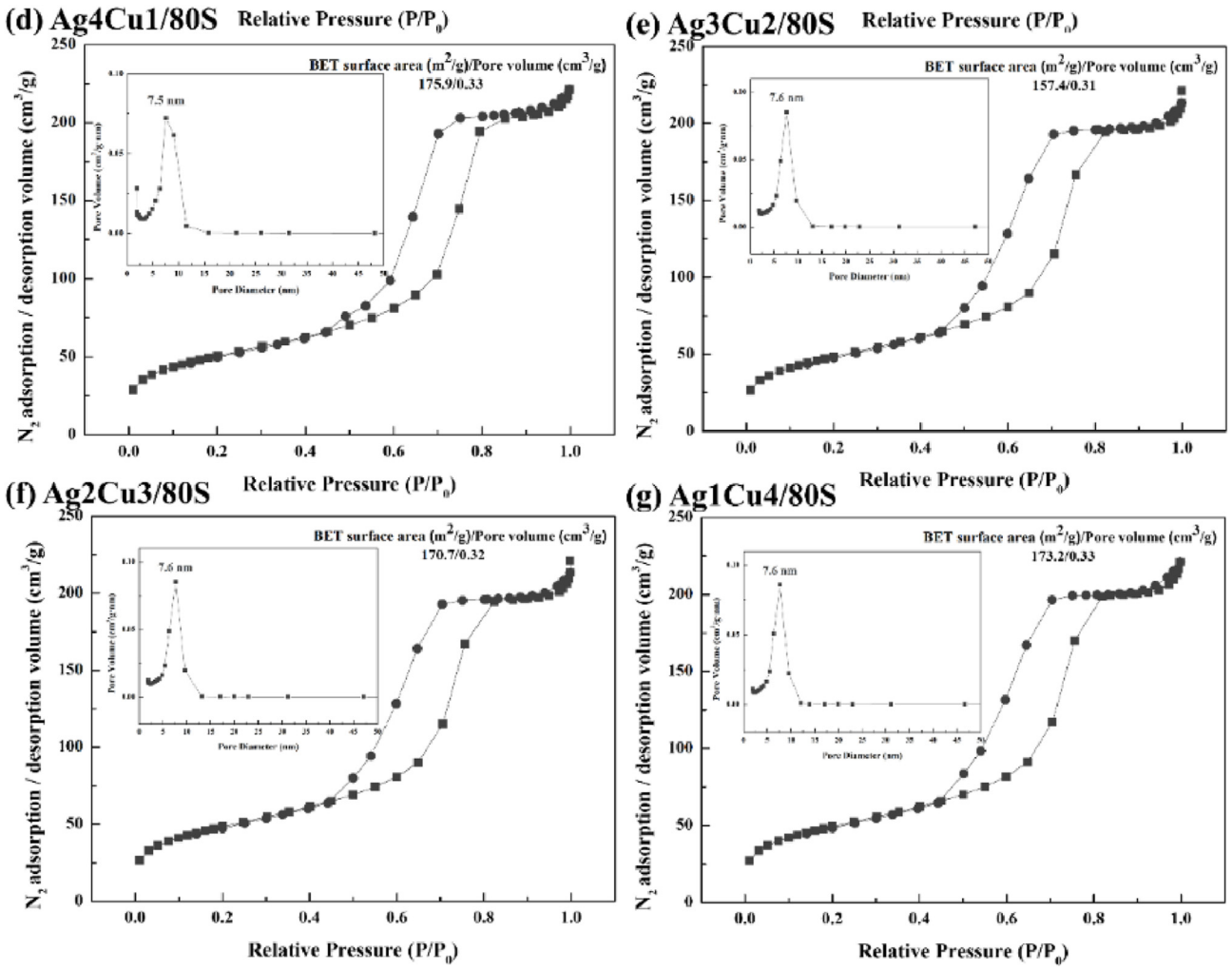


**Figure 3** (*continued*).

**Table 1** The result of nitrogen adsorption/desorption isotherm and pore size distribution curve.

| | $S_{BET}$ ($m^2$/g) | The percentage of decrease $S_{BET}$ (%)[a] | $V_P$ ($cm^3$/g) | The percentage of decrease $V_P$ (%)[a] | Pore size (nm) |
|---|---|---|---|---|---|
| 80S | 294.1 | - | 0.51 | - | 7.6 |
| Ag5/80S | 154.9 | 47.3 | 0.33 | 35.3 | 7.4 |
| Cu5/80S | 150.2 | 48.9 | 0.35 | 31.4 | 9.1 |
| Ag4Cu1/80S | 175.9 | 40.2 | 0.33 | 35.3 | 7.5 |
| Ag3Cu2/80S | 157.4 | 46.5 | 0.31 | 39.2 | 7.6 |
| Ag2Cu3/80S | 170.7 | 41.9 | 0.32 | 37.3 | 7.6 |
| Ag1Cu4/80S | 173.2 | 41.1 | 0.33 | 35.3 | 7.6 |

[a] deceased percentage compared to that of 80S.

copper was observed in micrographs as black dots or shadows (Fig. 4), which agreed with the findings by Sánchez-Salcedo et al.[24]

## Ion release of AgCu/80S

The release of ions was considered the determinant for antibacterial activities,[32] where the BHI medium base was employed for the growth of *E. faecalis*. Proteins or amino acids were regarded as the key component to release the metal ions from metal-containing MBGs.[33] Thus, the liberation of silver and copper from the AgCu/80S materials was detected using an ICP-MS (Fig. 5). The quantities of silver ions released for materials containing silver (e.g., Ag5/80S, Ag4Cu1/80S, Ag3Cu2/80S, Ag2Cu3/80S, and Ag1Cu4/80S) were 102.0 ± 0.1, 96.5 ± 0.2, 112.6 ± 0.1, 70.0 ± 0.0, and 33.8 ± 0.1 ppm, respectively. On the other hand, for those

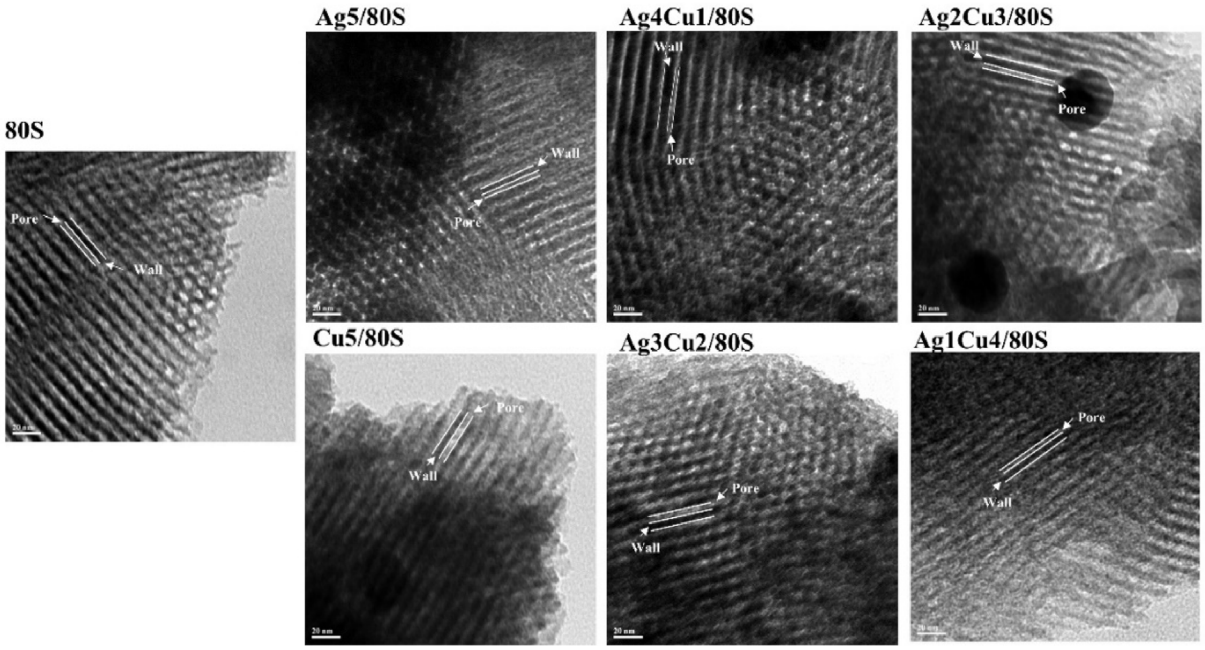


**Figure 4** TEM micrographs of 80S, Ag5/80S, Cu5/80S, Ag4Cu1/80S, Ag3Cu2/80S, Ag2Cu3/80S and Ag1Cu4/80S. The scale bar down left displayed 20 nm.

containing copper, the quantities of copper were determined as 123.8 ± 0.2, 202.8 ± 0.0, 205.8 ± 0.1, 131.2 ± 0.1, and 363.9 ± 0.0 ppm, respectively. The quantity of silver released from Ag3Cu2/80S was relatively higher than others, speculating a phenomenon of copper-enhanced silver release.

## Antibacterial activity of AgCu/80S

To examine the antibacterial activities of AgCu/80S materials, disk diffusion assays against *E. faecalis* ATCC 29212 were performed (Fig. 6). Neither 80S nor Cu5/80S exhibited an inhibition zone, while the materials containing silver showed inhibition zone, with diameters of 8.21 ± 0.06, 9.92 ± 0.04, 9.09 ± 0.09, 8.64 ± 0.04, and 8.39 ± 0.07 mm for Ag1Cu4/80S, Ag2Cu3/80S, Ag3Cu2/80S, Ag4Cu1/80S, and Ag5/80S, respectively. To further understand the antibacterial kinetics of AgCu/80S against *E. faecalis*, the bacterial growth curves were recorded, where the MICs were also determined, with the colony-forming assays for the MBCs (Fig. 7). No inhibition was found for *E. faecalis* with Cu5/80S (Fig. 7a and b), illustrating that the copper released from Cu5/80S possessed no antibacterial activity. The MICs of Ag1Cu4/80S, Ag2Cu3/80S, Ag3Cu2/80S, Ag4Cu1/80S, and Ag5/80S against *E. faecalis* were all found as 20 mg/mL (Table 2), with delayed growth at concentrations lower than 20 mg/mL noticed in the growth curves (Fig. 7c, e, 7g, 7i and 7k). Notably, the dose-dependent trends of delayed growth were found for Ag2Cu3/80S, Ag3Cu2/80S, Ag4Cu1/80S, and Ag5/80S (Fig. 7e, g, 7i and 7k), with growth postponed to approximately 6h, 8h, and 12h at 2.5, 5, and 10 mg/mL, respectively. Additionally, the MBCs of Ag1Cu4/80S, Ag2Cu3/80S, Ag3Cu2/80S, Ag4Cu1/80S, and Ag5/80S against *E. faecalis* ranged from 20 to >20 mg/mL, with the lowest MBCs observed for Ag2Cu3/80S and Ag3Cu2/80S, where the silver content of Ag3Cu2/80S was found as the highest among the materials in this study (Fig. 5). The findings implied that the AgCu/80S synthesized in this study possessed antibacterial activities, whereas the Ag2Cu3/80S and Ag3Cu2/80S demonstrated better efficacy among these.

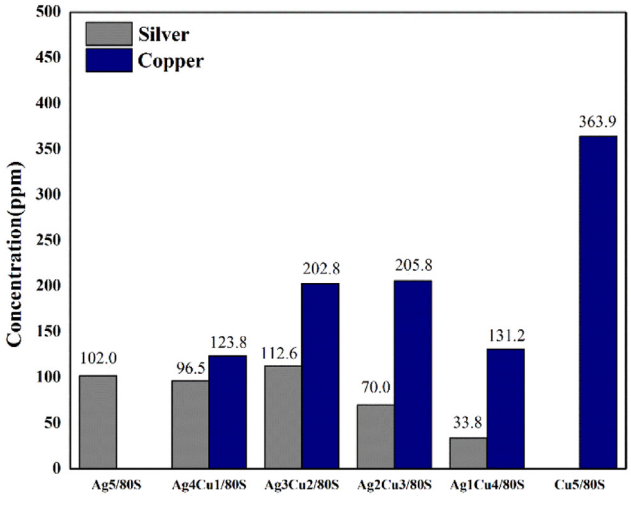


**Figure 5** ICP-MS results of the inspired Ag5/80S, Ag4Cu1/80S, Ag3Cu2/80S, Ag2Cu3/80S, Ag1Cu4/80S, and Cu5/80S in BHI broth.

## Discussion

The crystal phases found in this study agreed with the previous efforts (Fig. 1).[24,29,34,35] Besides, compared to the

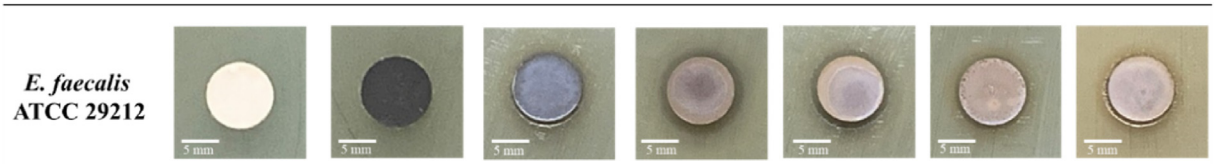


| Disk | 80S | Cu5/80S | Ag1Cu4/80S | Ag2Cu3/80S | Ag3Cu2/80S | Ag4Cu1/80S | Ag5/80S |
|---|---|---|---|---|---|---|---|
| Diameter (mm) | - | - | 8.21±0.06 | 9.92±0.04 | 9.09±0.09 | 8.64±0.04 | 8.39±0.07 |

**Figure 6** Disk diffusion of 80S, Cu5/80S, Ag1Cu4/80S, Ag2Cu3/80S, Ag3Cu2/80S, Ag4Cu1/80S, and Ag5/80S against *E. faecalis* ATCC29212. The scale bar down left displayed 5 mm.

previous report by Huang et al.,[29] the analyses revealed a weaker crystallization for calcium silicate ($Ca_2SiO_4$) on planes of (301) with the modification of preparation to shorten the aging time from 3 days to 1 day and increase the temperature from 25 to 100 °C, indicating the materials we synthesized a bioglass. Our UV–vis results also agreed with the findings in XRD for copper (Fig. 2), with no signal found in UV–vis spectra and weak intensity of copper crystallization. Similar findings for silver nanoparticles were described in several studies.[36,37] In the previous study,[25] Wu et al. synthesized Cu-MBG through the sol–gel method, denoted as 1Cu-MBG, 2Cu-MBG, and 5Cu-MBG, with their respective Si/Ca/P/Cu molar ratios being 80/(15-x)/5/x (where x = 0, 1, 2, and 5). The surface area, pore volume, and pore size of their MBG were reported as 539 $m^2/g$, 0.60 $cm^3/g$, and 5.2 nm, respectively. For 1Cu-MBG, the corresponding values were 310 $m^2/g$, 0.36 $cm^3/g$, and 4.2 nm; for 2Cu-MBG were reported as 353 $m^2/g$, 0.34 $cm^3/g$, and 3.8 nm; for 5Cu-MBG were reported as 334 $m^2/g$, 0.44 $cm^3/g$, and 4.7 nm, exhibiting a type IV H1 isotherm curve hysteresis loop characteristics. Similar findings were reported by Sánchez-Salcedo et al.,[24] who synthesized mesoporous bioactive glasses containing silver (MBG-0.15Ag, MBG-0.3Ag, and MBG-1Ag), with also a type IV H1 isotherm curve hysteresis loop characteristics. As the mole ratio of silver increased, surface area, pore volume, and pore size decreased, suggesting the incorporation of silver in materials. Their study also revealed the XRD results of silver (Ag) at $2\theta$ = 38.1°, 44.3°, 64.5°, and 77.1°, with the crystal planes of (111), (200), (220), and (311), respectively. Even with the modification of preparation, no notable difference was found between the materials synthesized in this study and by Huang et al.[29]

In the previous study, Baino et al. conducted the synthesis of mesoporous bioactive glasses containing copper via the sol–gel method in 2018,[38] with a composition of $57SiO_2$–$32CaO$–$6Na_2O$–$3Al_2O_3$-x$CuO$ mol%, where x = 2, 5, denoted as SCNA-2Cu and SCNA-5Cu. The evaluation of Cu ion release in simulated body fluid revealed an increase in copper ion release over time for both groups, with SCNA-5Cu exhibiting the highest copper release. In another study, Huang et al. synthesized MBG-Ag through the sol–gel method and evaluated the released silver content in various media such as water, PBS, TSB, and taurine.[33] The results indicated differing silver concentrations, with the highest in Tau-Ag (272.90 ppm), followed by TSB-Ag. In a separate study, Huang et al. synthesized silver-containing copper mesoporous bioactive glass AgCu/80S using the sol–gel method.[29] The evaluation of silver and copper release showed similar silver release among the bimetallic groups, higher than Ag5/80S, while copper release increased with a higher copper ratio, suggesting that the simultaneous loading of two metals promotes an increase in silver release. The results of the copper-enhanced silver release agreed with the previous study,[29] where the antibacterial activity was also increased against methicillin-resistant *S. aureus* (MRSA). However, compared to their case, the preparation of materials in this study was modified, decreasing the crystal phase of $CaSiO_4$. The matrix for metal inspiration used in this study was BHI, where the protein content is more prosperous than that in TSB. The findings revealed the different ion-releasing activities between the materials synthesized in this study and by Huang et al.[29] Besides, Huang et al. synthesized AgCu/80S materials using a sol–gel method and evaluated their activity against methicillin-resistant *S. aureus*. The composition of Ag1Cu4/80S exhibited the best antibacterial activities, with the MIC and MBC of 5 and 10 mg/mL, respectively. With modifications of the material preparation, the AgCu/80S materials in this study displayed different activities against *E. faecalis* ATCC 29212, whereas the Ag2Cu3/80S and Ag3Cu2/80S showed the most extraordinary.

The textural findings in this study agreed with the previous study,[29] while the ion-releasing and antibacterial activities were different. It was speculated that the shorter time and higher temperature for material aging form a material closer to glass but with different ion-releasing and antibacterial activities. Further study of the AgCu/80S glasses would be needed to investigate the appropriate environment for ion release, bioactivities (including

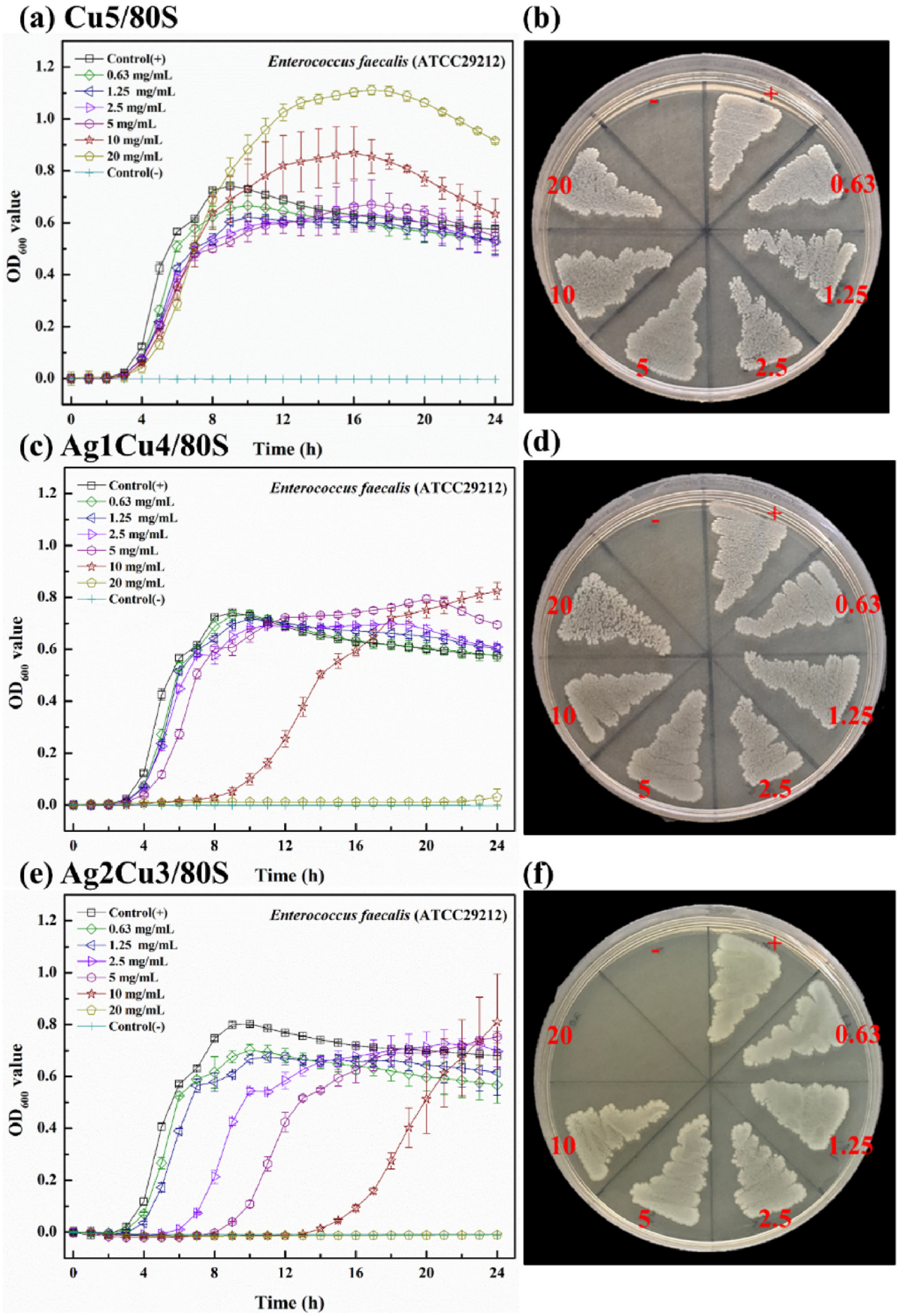


**Figure 7** The bacterial growth curve and colony forming tests for Cu5/80S (**a** and **b**), Ag1Cu4/80S (**c** and **d**), Ag2Cu3/80S (**e** and **f**), Ag3Cu2/80S (**g** and **h**), Ag4Cu1/80S (**i** and **j**), and Ag5/80S (**k** and **l**) against *E. faecalis* ATCC29212.

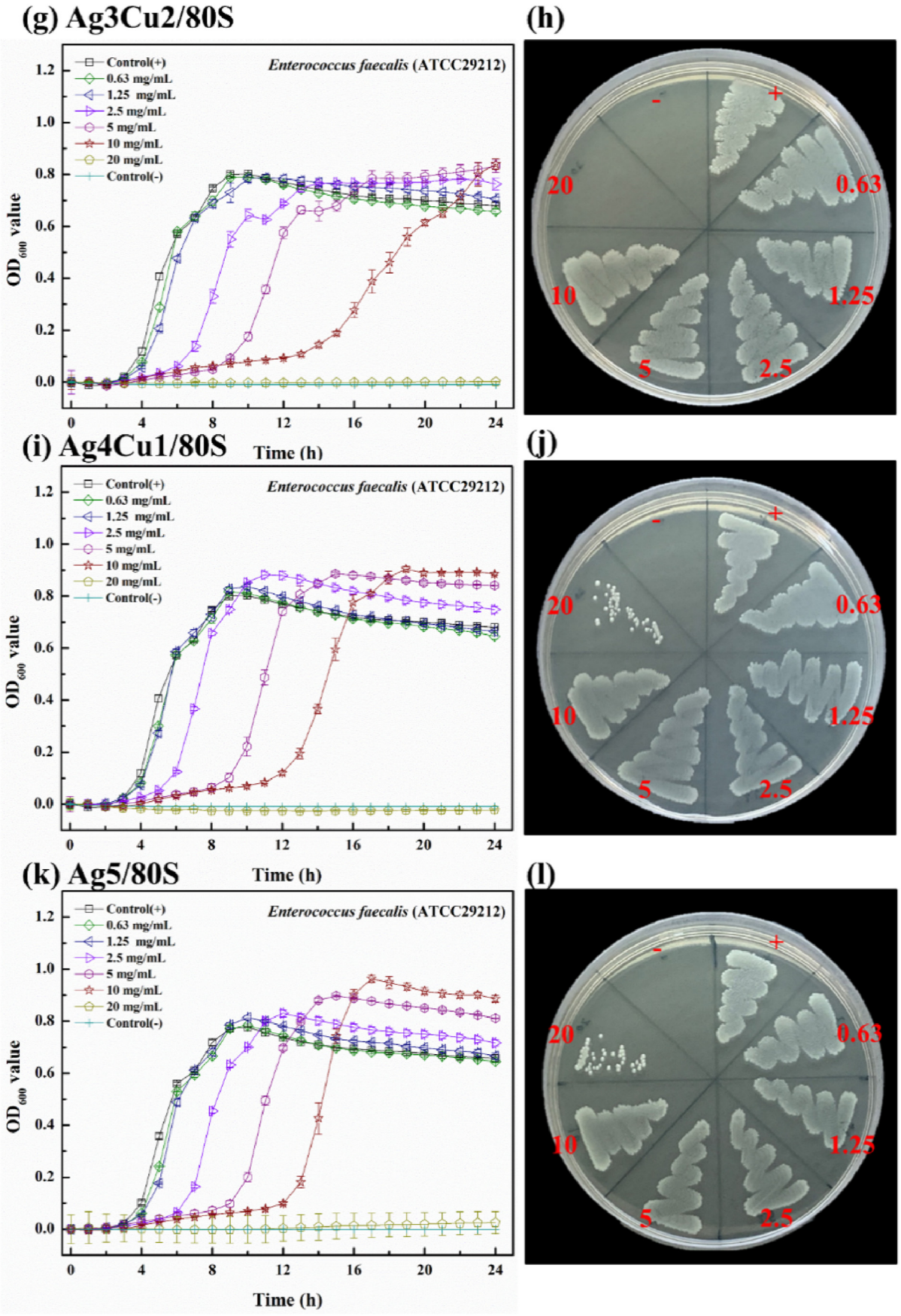


**Figure 7** (*continued*).

**Table 2** MICs and MBCs of AgCu/80S against *E. faecalis* ATCC29212.

| Material | Cu5/80S | Ag1Cu4/80S | Ag2Cu3/80S | Ag3Cu2/80S | Ag4Cu1/80S | Ag5/80S |
|---|---|---|---|---|---|---|
| MIC (mg/mL) | >20 | 20 | 20 | 20 | 20 | 20 |
| MBC (mg/mL) | >20 | >20 | 20 | 20 | >20 | >20 |

hydroxyapatite formation, cell proliferation, and osteoinduction), and its dental applications (bone formation and angiogenesis).

## Declaration of competing interest

The authors have no conflicts of interest relevant to this article.

## Acknowledgments

This work was funded by the research project of the National Science and Technology Council, Taiwan (NSTC 112-2320-B-214-009), the Chi-Mei Medical Center and Kaohsiung Medical University Research Foundation (112-CM-KMU-04), the Kaohsiung Medical University Research Foundation (KMU-M113003), and I-Shou University, Taiwan (ISU-112-02-03A and ISU112—S-03).

## References

1. Paredes-Vieyra J, Enriquez FJ. Success rate of single- versus two-visit root canal treatment of teeth with apical periodontitis: a randomized controlled trial. *J Endod* 2012;38:1164—9.
2. Kearney M, Cooper PR, Smith AJ, Duncan HF. Epigenetic approaches to the treatment of dental pulp inflammation and repair: opportunities and obstacles. *Front Genet* 2018;9:311.
3. Alghamdi F, Shakir M. The influence of Enterococcus faecalis as a dental root canal pathogen on endodontic treatment: a systematic review. *Cureus* 2020;12:e7257.
4. Pourhajibagher M, Ghorbanzadeh R, Bahador A. Culture-dependent approaches to explore the prevalence of root canal pathogens from endodontic infections. *Braz Oral Res* 2017;31:e108.
5. Bansal R, Jain A. An insight into patient's perceptions regarding root canal treatment: a questionnaire-based survey. *J Fam Med Prim Care* 2020;9(2):1020—7.
6. Murray PE. Review of guidance for the selection of regenerative endodontics, apexogenesis, apexification, pulpotomy, and other endodontic treatments for immature permanent teeth. *Int Endod J* 2023;56(Suppl 2):188—99.
7. Bakhtiar H, Nekoofar MH, Aminishakib P, et al. Human pulp responses to partial pulpotomy treatment with TheraCal as compared with Biodentine and ProRoot MTA: a clinical trial. *J Endod* 2017;43:1786—91.
8. El-Fiqi A, Mandakhbayar N, Jo SB, Knowles JC, Lee JH, Kim HW. Nanotherapeutics for regeneration of degenerated tissue infected by bacteria through the multiple delivery of bioactive ions and growth factor with antibacterial/angiogenic and osteogenic/odontogenic capacity. *Bioact Mater* 2021;6:123—36.
9. Sakko M, Tjaderhane L, Rautemaa-Richardson R. Microbiology of root canal infections. *Prim Dent J* 2016;5:84—9.
10. Rocas IN, Siqueira Jr JF, Santos KR. Association of Enterococcus faecalis with different forms of periradicular diseases. *J Endod* 2004;30:315—20.
11. Namour M, Theys S. Pulp revascularization of immature permanent teeth: a review of the literature and a proposal of a new clinical protocol. *Sci World J* 2014;2014:737503.
12. Zanini M, Hennequin M, Cousson PY. A review of criteria for the evaluation of pulpotomy outcomes in mature permanent teeth. *J Endod* 2016;42:1167—74.
13. Hilton TJ, Ferracane JL, Mancl L. Northwest Practice-based Research Collaborative in Evidence-based Dentistry (NWP). Comparison of $Ca(OH)_2$ with MTA for direct pulp capping: a PBRN randomized clinical trial. *J Dent Res* 2013;92(Suppl 7):16S—22S.
14. da Rosa WLO, Cocco AR, Silva TMD, et al. Current trends and future perspectives of dental pulp capping materials: a systematic review. *J Biomed Mater Res B Appl Biomater* 2018;106:1358—68.
15. Nowicka A, Wilk G, Lipski M, Kolecki J, Buczkowska-Radlinska J. Tomographic evaluation of reparative dentin formation after direct pulp capping with $Ca(OH)_2$, MTA, Biodentine, and dentin bonding system in human teeth. *J Endod* 2015;41:1234—40.
16. Shah A, Peacock R, Eliyas S. Pulp therapy and root canal treatment techniques in immature permanent teeth: an update. *Br Dent J* 2022;232:524—30.
17. Kim RJ, Kim MO, Lee KS, Lee DY, Shin JH. An in vitro evaluation of the antibacterial properties of three mineral trioxide aggregate (MTA) against five oral bacteria. *Arch Oral Biol* 2015;60:1497—502.
18. Esteki P, Jahromi MZ, Tahmourespour A. In vitro antimicrobial activity of mineral trioxide aggregate, Biodentine, and calcium-enriched mixture cement against Enterococcus faecalis, Streptococcus mutans, and Candida albicans using the agar diffusion technique. *Dent Res J* 2021;18:3.
19. Schumacher M, Habibovic P, van Rijt S. Mesoporous bioactive glass composition effects on degradation and bioactivity. *Bioact Mater* 2021;6:1921—31.
20. Wu C, Chang J. Mesoporous bioactive glasses: structure characteristics, drug/growth factor delivery and bone regeneration application. *Interface Focus* 2012;2:292—306.
21. Crisan CM, Mocan T, Manolea M, Lasca LI, Tăbăran F-A, Mocan L. Review on silver nanoparticles as a novel class of antibacterial solutions. *Appl Sci* 2021;11:1120.
22. Qian G, Zhang L, Liu X, Wu S, Peng S, Shuai C. Silver-doped bioglass modified scaffolds: a sustained antibacterial efficacy. *Mater Sci Eng C* 2021;129:112425.
23. Ciraldo FE, Liverani L, Gritsch L, Goldmann WH, Boccaccini AR. Synthesis and characterization of silver-doped mesoporous bioactive glass and its applications in conjunction with electrospinning. *Materials* 2018;11:692.
24. Sanchez-Salcedo S, Garcia A, Gonzalez-Jimenez A, Vallet-Regi M. Antibacterial effect of 3D printed mesoporous bioactive glass scaffolds doped with metallic silver nanoparticles. *Acta Biomater* 2023;155:654—66.
25. Wu C, Zhou Y, Xu M, et al. Copper-containing mesoporous bioactive glass scaffolds with multifunctional properties of

angiogenesis capacity, osteostimulation and antibacterial activity. *Biomaterials* 2013;34:422—33.
26. Vasiliev G, Kubo AL, Vija H, et al. Synergistic antibacterial effect of copper and silver nanoparticles and their mechanism of action. *Sci Rep* 2023;13:9202.
27. Hao Z, Wang M, Cheng L, Si M, Feng Z, Feng Z. Synergistic antibacterial mechanism of silver-copper bimetallic nanoparticles. *Front Bioeng Biotechnol* 2023;11:1337543.
28. Li YJ, Wong KW, Huang YC, Chien CS, Shih CJ. Evaluation of in vitro bioactivity and angiogenesis-promoting effect for mesoporous bioactive glass codoped with copper and silver. *J Non-Cryst Solids* 2023;613:122371.
29. Huang YC, Lin TY, Huang SC, Yang TY, Shih CJ. Copper-enhanced silver releasing from bimetal-containing bioactive glass (AgCu/80S) elicits antibacterial efficacy against drug-resistant *Staphylococcus aureus*. *J Non-Cryst Solids* 2022;584:121509.
30. Huang X, El-Sayed MA. Gold nanoparticles: optical properties and implementations in cancer diagnosis and photothermal therapy. *J Adv Res* 2010;1:13—28.
31. Gelb LD, Gubbins K. Characterization of porous glasses: simulation models, adsorption isotherms, and the Brunauer—Emmett—Teller analysis method. *Langmuir* 1998;14:2097—111.
32. Godoy-Gallardo M, Eckhard U, Delgado LM, et al. Antibacterial approaches in tissue engineering using metal ions and nanoparticles: from mechanisms to applications. *Bioact Mater* 2021;6:4470—90.
33. Huang YC, Yang TY, Chen BX, Kung JC, Shih CJ. Evaluation of antibacterial effects of matrix-induced silver ions against antibiotic-resistant ESKAPE pathogens. *Pharmaceuticals* 2021;14:1094.
34. Mortazavi S, Rahsepar M, Hosseinzadeh S. Modification of mesoporous structure of silver-doped bioactive glass with antibacterial properties for bone tissue applications. *Ceram Int* 2022;48:8276—85.
35. Wang X, Cheng F, Liu J, et al. Biocomposites of copper-containing mesoporous bioactive glass and nanofibrillated cellulose: biocompatibility and angiogenic promotion in chronic wound healing application. *Acta Biomater* 2016;46:286—98.
36. Gondwal M, Joshi nee Pant G. Synthesis and catalytic and biological activities of silver and copper nanoparticles using *Cassia occidentalis*. *Int J Biomater* 2018;2018:6735426.
37. Kalaivani R, Maruthupandy M, Muneeswaran T, et al. Synthesis of chitosan mediated silver nanoparticles (AgNPs) for potential antimicrobial applications. *Front Lab Med* 2018;2:30—5.
38. Baino F, Potestio I, Vitale-Brovarone C. Production and physicochemical characterization of Cu-doped silicate bioceramic scaffolds. *Materials* 2018;11:1524.